Strong anharmonic and quantum effects in $Pm\bar{3}n$ AlH_3 under high pressure: A first-principles study

Pugeng Hou [1], Francesco Belli,[2,3] Raffaello Bianco,[3] and Ion Errea [2,3,4]

[1] *College of Science, Northeast Electric Power University, Changchun Road 169, 132012 Jilin, People's Republic of China*

[2] *Fisika Aplikatua Saila, Gipuzkoako Ingeniaritza Eskola, University of the Basque Country (UPV/EHU), Europa Plaza 1, 20018 Donostia/San Sebastián, Spain*

[3] *Centro de Física de Materiales (CSIC-UPV/EHU), Manuel de Lardizabal Pasealekua 5, 20018 Donostia/San Sebastián, Spain*

[4] *Donostia International Physics Center (DIPC), Manuel de Lardizabal Pasealekua 4, 20018 Donostia/San Sebastián, Spain*

(Received 29 January 2021; revised 26 March 2021; accepted 6 April 2021; published 29 April 2021)

Motivated by the absence of experimental superconductivity in the metallic $Pm\bar{3}n$ phase of AlH_3 despite the predictions, we reanalyze its vibrational and superconducting properties at pressures $P \geqslant 99$ GPa making use of first-principles techniques. In our calculations based on the self-consistent harmonic approximation method that treats anharmonicity beyond perturbation theory, we predict a strong anharmonic correction to the phonon spectra and demonstrate that the superconducting critical temperatures predicted in previous calculations based on the harmonic approximation are strongly suppressed by anharmonicity. The electron-phonon coupling concentrates on the lowest-energy hydrogen-character optical modes at the X point of the Brillouin zone. As a consequence of the strong anharmonic enhancement of their frequency, the electron-phonon coupling is suppressed by at least 30%. The suppression in λ makes T_c smaller than 4.2 K above 120 GPa, which is well consistent with the experimental evidence. Our results underline that metal hydrides with hydrogen atoms in interstitial sites are subject to huge anharmonic effects.

DOI: 10.1103/PhysRevB.103.134305

I. INTRODUCTION

Motivated by the quest for metallic and superconducting hydrogen at very high pressures [1], a combination of first-principles structural predictions and calculations of the electron-phonon interaction has led in the last years to the prediction of many superconducting hydrides with high values of the superconducting critical temperature T_c [2–21]. Even if the observation of high T_c in pure hydrogen remains still elusive, although optical evidence of the probably superconducting atomic phase [22,23] has been reported [24], it is now an experimental fact that room-temperature superconductivity is possible in hydrogen-rich "superhydride" compounds. Critical temperatures above 200 K have been observed in sulfur [25], lanthanum [26,27], and yttrium [28–30] superhydrides at pressures exceeding 100 GPa. A mixture of C-H-S has finally reached room-temperature superconductivity at pressures above 250 GPa [31], showing that there is lots of room for further increase in T_c among ternary compounds [19]. The role of theoretical first-principles calculations in all these experimental discoveries should be highlighted. For instance, the discoveries of high-T_c superconductivity in sulfur, lanthanum, and yttrium hydrides had been anticipated by *ab initio* calculations [14,15,17,32].

The standard procedure in these *ab initio* calculations relies on a classical treatment of the ions: The predicted structures are minima of the Born-Oppenheimer energy surface (BOES), and the phonons entering the superconducting equations are estimated assuming a harmonic expansion of the BOES around these crystal configurations. However, this classical (or harmonic) approach often completely breaks down as it neglects the quantum contribution from the kinetic term of the nuclei Hamiltonian to the energy and the phonon frequencies. The latter is large in hydrogen-based compounds due to the lightness of H atoms. Consequently, the T_c from classical harmonic calculations [11,18,32] usually differ from the experimental values [25,27,32]. In fact, the anharmonic correction to the phonon frequencies imposed by the large ionic quantum fluctuations strongly renormalizes the superconducting critical temperatures in hydrogen-based superconductors, yielding T_c's in close agreement with experiments [33–37]. Furthermore, quantum anharmonic effects also explain the stabilization of the crystal structures of superhydrides observed experimentally, as, otherwise, these structures would not be the ground state [35,36].

In the literature of superconducting hydrides, AlH_3 deserves a remarkable position as it was one of the first metallic hydrogen-based compounds synthesized at high pressures [32] after having been predicted theoretically by crystal structure prediction methods [38]. Despite having been predicted to be a superconductor at 24 K at 110 GPa in the $Pm\bar{3}n$ phase within standard harmonic calculations, experimentally no superconductivity was observed down to 4 K over the 120–164 GPa pressure range [32]. It was later suggested that anharmonicity was responsible for the suppression of T_c [39]. Even if this seemed to close the debate on the experimental and theoretical disagreement, the perturbative treatment of anharmonicity followed in Ref. [39] for this system seems questionable, as the anharmonic self-energy for some particular modes was estimated to be as high as the phonon frequencies themselves. In these conditions, perturbative approaches may lead to strong errors in the estimation of the

renormalized phonon frequencies [40]. Furthermore, anharmonic corrections were only estimated for few modes at only one pressure. A deeper analysis based not on a perturbative method is thus required to confirm that anharmonicity is responsible for the suppression of T_c in AlH_3.

In this paper we present a thorough first-principles analysis of the full anharmonic phonon spectra of $Pm\bar{3}n$ AlH_3 in a wide pressure range based on the variational stochastic self-consistent harmonic approximation (SSCHA) method [33,41–43]. The calculated superconducting critical temperature is strongly suppressed by anharmonicity in the whole pressure range, in agreement with the absence of superconductivity in the 120–164 GPa pressure range above 4 K, confirming the suggestion made in Ref. [39]. The paper is organized as follows: Sec. II describes the theoretical framework of our anharmonic *ab initio* calculations, Sec. III overviews the computational details of our calculations, Sec. IV presents the results of the calculations, and Sec. V summarizes the main conclusions of this work.

II. METHODOLOGY

In the following, we briefly review the SSCHA method [33,41–43] used for the calculation of anharmonic phonon frequencies, as well as the theoretical framework followed for estimating the superconducting critical temperature.

A. The stochastic self-consistent harmonic approximation

The SSCHA [33,41–43] is a quantum variational method that minimizes the free energy of the system calculated with a trial density matrix $\tilde{\rho}_{\mathcal{R},\Phi}$:

$$\mathcal{F}[\tilde{\rho}_{\mathcal{R},\Phi}] = \langle K + V(\boldsymbol{R})\rangle_{\tilde{\rho}_{\mathcal{R},\Phi}} - TS[\tilde{\rho}_{\mathcal{R},\Phi}]. \tag{1}$$

Here, K is the ionic kinetic energy, $V(\boldsymbol{R})$ is the full Born-Oppenheimer potential, T is the temperature, and $S[\tilde{\rho}_{\mathcal{R},\Phi}]$ is the entropy calculated with the trial density matrix. In the SSCHA the density matrix is parametrized with centroid positions $\boldsymbol{\mathcal{R}}$, which determine the average ionic positions, and auxiliary force constants $\boldsymbol{\Phi}$, which are related to the broadening of the ionic wave functions around $\boldsymbol{\mathcal{R}}$. Thus, minimizing $\mathcal{F}[\tilde{\rho}_{\mathcal{R},\Phi}]$ with respect to $\boldsymbol{\mathcal{R}}$ and $\boldsymbol{\Phi}$, a good variational approximation of the free energy can be obtained without approximating the Born-Oppenheimer potential. This free energy can be used to estimate thermodynamic magnitudes, such as the pressure, including the effects of ionic quantum fluctuations [42]. These effects are neglected if the pressure is estimated instead from $V(\boldsymbol{R})$, which is the standard procedure.

Phonon frequencies within the SSCHA should be calculated from the dynamical extension of the theory [41,44,45]. In this framework, phonon frequencies at the $\boldsymbol{q}$ point of the Brillouin zone (BZ) appear as peaks of the one-phonon spectral function

$$\sigma(\boldsymbol{q},\Omega) = -\frac{\Omega}{\pi}\,\mathrm{Im}\mathrm{Tr}[\boldsymbol{G}(\boldsymbol{q},\Omega + i0^+)], \tag{2}$$

where $\boldsymbol{G}(\boldsymbol{q},z)$ is the Fourier transform of the Green's function for the variable $\sqrt{M_a}(R^a - \mathcal{R}^a_{\mathrm{eq}})$, which is related to the correlation between displacements of atoms from the centroid positions at equilibrium. The index a labels both an atom and a Cartesian direction, and M_a is the mass of atom a. 0^+ is a small positive number. We calculate the spectral function both keeping the full energy dependence of the phonon self-energy and within the so-called Lorentzian approximation (see Ref. [46] for details). In the latter case, the spectral function has well-defined Lorentzian line shape, with well-defined peaks at the $\Omega_\mu(\boldsymbol{q})$ frequencies.

In the $\Omega \to 0$ static limit, the peaks coincide with the $\Omega_\mu(\boldsymbol{q})$ frequencies, with $\Omega^2_\mu(\boldsymbol{q})$ being the eigenvalues of the Fourier transform of the free-energy Hessian matrix

$$D^{(\mathrm{F})}_{ab} = \frac{1}{\sqrt{M_a M_b}}\left[\frac{\partial^2 F}{\partial\mathcal{R}^a\partial\mathcal{R}^b}\right]_{\boldsymbol{\mathcal{R}}_{\mathrm{eq}}}. \tag{3}$$

In Eq. (3), F is assumed to be the free energy at the minimum, and $\boldsymbol{\mathcal{R}}_{\mathrm{eq}}$ are the centroid positions that minimize Eq. (1). As the phonon frequencies obtained in this static limit are determined by the free-energy Hessian, $\Omega_\mu(\boldsymbol{q})$ imaginary frequencies point to lattice instabilities in the quantum anharmonic energy landscape.

B. Calculation of the superconducting transition temperature

We evaluate T_c with the Allen-Dynes [47] modified McMillan equation,

$$T_c = \frac{f_1 f_2\,\omega_{\log}}{1.2}\exp\left[-\frac{1.04(1+\lambda)}{\lambda - \mu^*(1+0.62\lambda)}\right], \tag{4}$$

where λ is the electron-phonon coupling constant and μ^* is a parameter usually named the Coulomb pseudopotential [48]. This equation has led to T_c values in rather good agreement with experiments in superhydrides [36] despite its simplicity. λ is defined as the first reciprocal moment of the electron-phonon Eliashberg function $\alpha^2F(\omega)$,

$$\lambda = 2\int_0^\infty d\omega\frac{\alpha^2F(\omega)}{\omega}. \tag{5}$$

Similarly,

$$\omega_{\log} = \exp\left(\frac{2}{\lambda}\int d\omega\frac{\alpha^2F(\omega)}{\omega}\ln\omega\right), \tag{6}$$

$$f_1 = \left[1 + (\lambda/\Lambda_1)^{3/2}\right]^{1/3}, \tag{7}$$

$$f_2 = 1 + \frac{(\bar{\omega}_2/\omega_{\log} - 1)\lambda^2}{\lambda^2 + \Lambda_2^2} \tag{8}$$

are also determined with $\alpha^2F(\omega)$. The Λ_1, Λ_2, and $\bar{\omega}_2$ parameters entering the equations above are given by

$$\Lambda_1 = 2.46(1 + 3.8\mu^*), \tag{9}$$

$$\Lambda_2 = 1.82(1 + 6.3\mu^*)(\bar{\omega}_2/\omega_{\log}), \tag{10}$$

$$\bar{\omega}_2 = \left[\frac{2}{\lambda}\int d\omega\alpha^2F(\omega)\omega\right]^{1/2}. \tag{11}$$

We calculate the Eliashberg function as

$$\alpha^2F(\omega) = \frac{1}{2\pi N(0)N_q}\sum_{\mu\boldsymbol{q}}\frac{\gamma_\mu(\boldsymbol{q})}{\omega_\mu(\boldsymbol{q})}\delta[\omega - \omega_\mu(\boldsymbol{q})], \tag{12}$$

where

$$\gamma_\mu(\boldsymbol{q}) = \frac{\pi}{N_k}\sum_{\boldsymbol{k}nm}\sum_{\bar{a}\bar{b}}\frac{\epsilon^{\bar{a}}_\mu(\boldsymbol{q})\epsilon^{\bar{b}}_\mu(\boldsymbol{q})^*}{\sqrt{M_{\bar{a}}M_{\bar{b}}}} d^{\bar{a}}_{\boldsymbol{k}n,\boldsymbol{k}+\boldsymbol{q}m} d^{\bar{b}*}_{\boldsymbol{k}n,\boldsymbol{k}+\boldsymbol{q}m} \times \delta(\varepsilon_{\boldsymbol{k}n})\delta(\varepsilon_{\boldsymbol{k}+\boldsymbol{q}m}) \quad (13)$$

is the phonon linewidth associated with the electron-phonon interaction of the mode μ at wave vector $\boldsymbol{q}$. In Eqs. (12) and (13), $d^{\bar{a}}_{\boldsymbol{k}n,\boldsymbol{k}+\boldsymbol{q}m} = \langle \boldsymbol{k}n|\, \delta V_{\rm KS}/\delta R^{\bar{a}}(\boldsymbol{q})\, |\boldsymbol{k}+\boldsymbol{q}m\rangle$, where $|\boldsymbol{k}n\rangle$ is a Kohn-Sham state with energy $\varepsilon_{\boldsymbol{k}n}$ measured from the Fermi level, $V_{\rm KS}$ is the Kohn-Sham potential, and $R^{\bar{a}}(\boldsymbol{q})$ is the Fourier-transformed displacement of atom $\bar{a}$; N_k and N_q are the number of electron and phonon momentum points used for the BZ sampling; $N(0)$ is the density of states at the Fermi level; and $\omega_\mu(\boldsymbol{q})$ and $\epsilon^{\bar{a}}_\mu(\boldsymbol{q})$ represent phonon frequencies and polarization vectors. The combined atom and Cartesian indices with a bar ($\bar{a}$) only run for atoms inside the unit cell. In this paper, the Eliashberg function is calculated both at the harmonic and anharmonic levels, respectively, by plugging into Eqs. (12) and (13) the harmonic phonon frequencies and polarization vectors or their anharmonic counterparts obtained diagonalizing $\boldsymbol{D}^{(\rm F)}$.

III. COMPUTATIONAL DETAILS

Electronic properties are computed using density functional theory (DFT) as implemented in the QUANTUM ESPRESSO package [49,50]. Ultrasoft pseudopotentials [51], including three electrons in the valence for Al, and a generalized gradient approximation for the exchange correlation potential are used [52]. The plane-wave basis cutoff is set to 80 Ry and to 800 Ry for the density. First BZ integrations are performed on a $24 \times 24 \times 24$ Monkhorst-Pack mesh, using a smearing parameter of 0.02 Ry. Harmonic phonon frequencies and electron-phonon matrix elements entering Eq. (13) are calculated within density functional perturbation theory (DFPT) [53].

The SSCHA variational minimization requires the calculation of forces in supercells. We calculate them within DFT in a $2 \times 2 \times 2$ supercell containing 64 atoms, yielding dynamical matrices on a commensurate $2 \times 2 \times 2$ grid. The difference between the harmonic and anharmonic dynamical matrices in the $2 \times 2 \times 2$ grid was interpolated to a $13 \times 13 \times 13$ grid. Adding the harmonic dynamical matrices in this fine grid to the result, the anharmonic dynamical matrices in the $13 \times 13 \times 13$ grid are obtained. Converging the value of the electron-phonon coupling constant required, indeed, a $13 \times 13 \times 13$ $\boldsymbol{q}$-point grid. A $60 \times 60 \times 60$ $\boldsymbol{k}$-point grid is used instead for the electronic integration in Eq. (13), and the Dirac deltas are approximated with Gaussian functions of 0.008 Ry width.

IV. RESULTS AND DISCUSSIONS

A. Pressure and crystal structure

$Pm\bar{3}n$ AlH_3 has a very high symmetry (see Fig. 1) with eight Al atoms in the corners and one Al atom in the center of the cubic unit cell. For each H atom there are 4 nearest Al neighbors at the same distance, while there are 12 equivalent H atom neighbors for each Al atom. Each H atom is located at an interstitial site, in the center of a regular tetrahedron formed by four Al atoms. All atomic positions are fixed by symmetry, and, as symmetry is imposed by the SSCHA, internal coordinates of the structure are not affected by quantum effects.

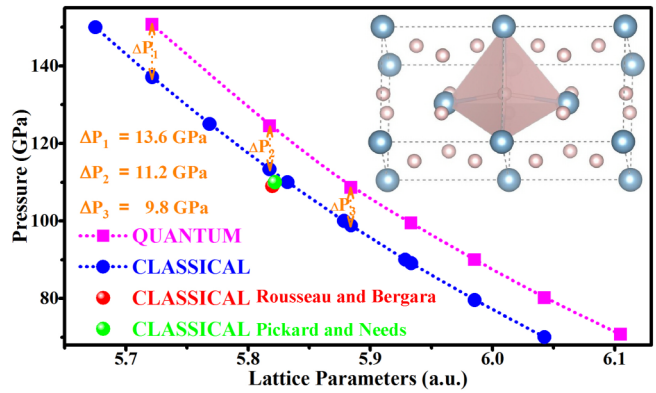

FIG. 1. Comparison between the classical and quantum pressures as a function of the lattice parameter. The classical pressure is obtained from the BOES, and the quantum pressure is obtained from the SSCHA free energy. Here are shown the differences at three pressures for the same lattice parameter. The crystal structure of $Pm\bar{3}n$ AlH_3 is shown as an illustration in the upper right corner, where the blue spheres represent Al atoms and the pink spheres represent H atoms. One of the tetrahedra surrounding hydrogen atoms is depicted. The classical calculations of Rousseau and Bergara [39] and Pickard and Needs [38] are also included.

However, the lattice parameter of the cubic structure is subject to quantum effects. In fact, as we show in Fig. 1 there are strong corrections to the pressure of the equation of states if ionic quantum effects are considered. For the same lattice parameter, the pressure obtained from the classical calculation based on the BOES (we will also refer to it as the harmonic pressure) is always about 10 GPa lower than the quantum result obtained with the SSCHA (we will also refer to it as the anharmonic pressure). This result is rather general among superhydrides, as similar quantum corrections on the pressure of about 10 GPa have been estimated for H_3S and LaH_{10} [35,36]. Figure 1 can be used conveniently to compare our results with previous classical calculations [32,39]. For instance, we clearly mark that the classical 110 and 125 GPa values correspond to 121.2 and 138.1 GPa in the quantum case, respectively. Consistently, in order to avoid any confusion, in the rest of the paper the pressure assigned to harmonic calculations will be the the classical one, while the quantum pressure will be assigned to quantum anharmonic calculations.

B. Phonon spectrum

The $Pm\bar{3}n$ phase of AlH_3 was observed experimentally above 100 GPa [32]. As shown in Fig. 2, approximately below this pressure the system develops phonon instabilities at the X point of the BZ in the classical harmonic calculation. In contrast, the anharmonic phonons obtained diagonalizing $\boldsymbol{D}^{(\rm F)}$ are always stable in the experimentally relevant pressure range. Therefore quantum anharmonic effects play a crucial role in stabilizing the $Pm\bar{3}n$ phase of AlH_3 around 100 GPa. This

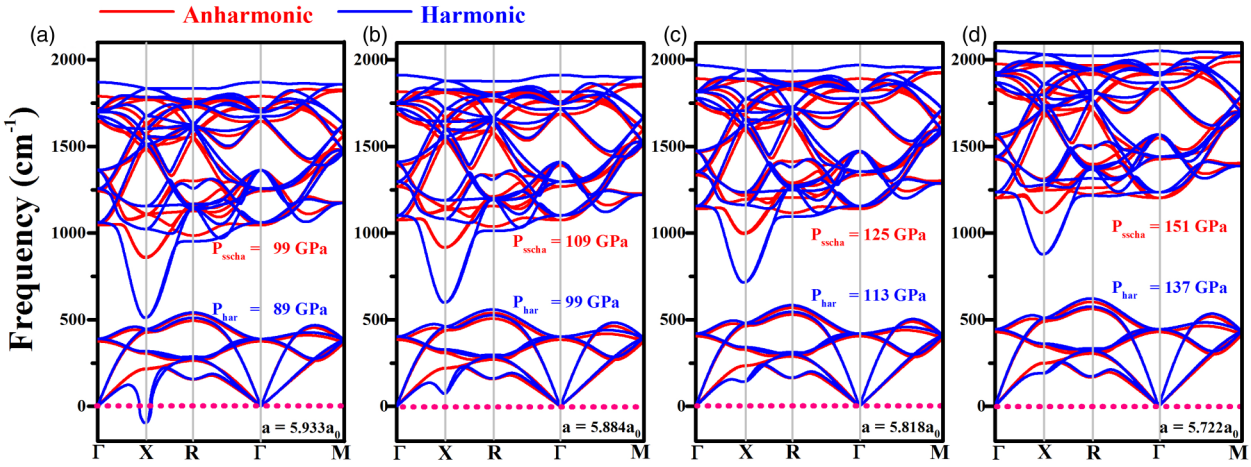

FIG. 2. Comparison between the harmonic (blue solid lines) and anharmonic (red solid lines) phonon spectra of the cubic high-symmetry $Pm\bar{3}n$ phase of AlH_3 for different lattice parameters. The anharmonic spectra are obtained from $\boldsymbol{D}^{(F)}$ and correspond to the static limit of the SSCHA dynamical theory. The pressure calculated classically (harmonic calculation) and with quantum effects (anharmonic calculation) is marked in each case. The regions of positive and negative frequencies, the latter of which represent imaginary frequencies, are separated with a pink dotted line.

phase remains dynamically stable at least down to 70 GPa. This means that even if below 100 GPa AlH_3 was found in an insulating $P1$ phase, the metallic phase may be metastable at lower pressures.

As shown in Fig. 2, the anharmonic correction leads to strong changes in the harmonic spectrum both for the low-energy acoustic and high-energy optical modes. Especially, the phonon frequencies at the X point of the BZ are strongly hardened by anharmonicity. Even if the anharmonic hardening of the phonon modes at the X point was already anticipated by the early calculations in Ref. [39], the fact that the anharmonic correction is of the order of the phonon frequency itself questions the perturbative approach followed previously. In fact, when using the 5.933a_0 lattice parameter, which corresponds to 99 GPa if quantum effects are considered, the instabilities apparent in the harmonic case completely hinder any perturbative approach.

In Fig. 3 we show the phonon spectral function $\sigma(\boldsymbol{q}, \Omega)$ calculated at the Γ and X points. These spectral functions can be directly probed by inelastic x-ray or neutron-scattering experiments [46]. We calculate the spectral function both keeping the full energy dependence of the phonon self-energy and within the so-called Lorentzian approximation (see Ref. [46] for details). While in the latter case the phonon peaks have, by construction, a Lorentzian line shape with a well-defined linewidth and clear peak position at the $\Omega_\mu(\boldsymbol{q})$ energies, in the former case quasiparticle peaks are not necessarily well determined. Despite the large anharmonic correction affecting the phonon frequencies, all phonon modes keep a well-defined Lorentzian line shape (see Fig. 3), also for the modes that suffer the largest correction at the X point. The linewidth of the phonons [half-width at half maximum (HWHM)] is very small for the phonon modes below 1100 cm^{-1}, less than 1 cm^{-1}, while for higher-energy modes it is in the range of ∼10 cm^{-1} (see Table I). It is remarkable that the phonon modes derived diagonalizing the free-energy Hessian $\boldsymbol{D}^{(F)}$ agree well with the peaks of the spectral function (see Table I), underlining that the phonon modes obtained in the static limit agree well with the peaks of the dynamical theory and are valid, for instance, to study superconducting properties.

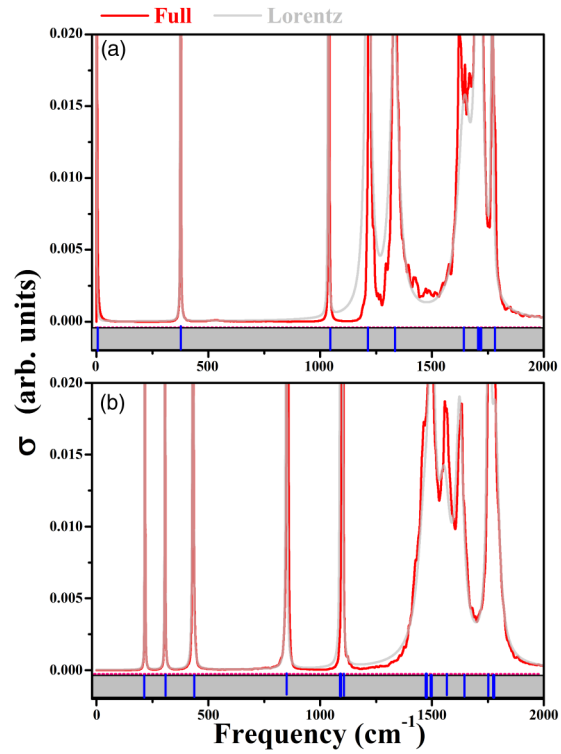

FIG. 3. Phonon spectral function $\sigma(\boldsymbol{q}, \Omega)$ of AlH_3 at 99 GPa (pressure calculated with anharmonic quantum effects), at (a) the Γ point and (b) the X point. The red line indicates the result obtained keeping the full energy dependence on the self-energy, and the gray line indicates the spectrum calculated in the Lorentzian approximation [41,46]. The centers of these Lorentzians define the anharmonic phonon frequencies. They are indicated with the blue short vertical lines in the lower panels of (a) and (b) with gray background.

TABLE I. The $\Omega_\mu(\boldsymbol{q})$ frequencies obtained from the free-energy Hessian $\boldsymbol{D}^{(\mathrm{F})}$, $\Omega_\mu(\boldsymbol{q})$ frequencies representing the location of the peaks in the spectral function in the Lorentzian approximation, and the anharmonic HWHM linewidth in the latter approximation for the phonon modes at the Γ and X points at 99 GPa (pressure calculated including quantum anharmonic effects).

Γ point				X point			
Modes	$\Omega_\mu(\boldsymbol{q})$	$\Omega_\mu(\boldsymbol{q})$	$\gamma_\mu^{\mathrm{anh}}(\boldsymbol{q})$	Modes	$\Omega_\mu(\boldsymbol{q})$	$\Omega_\mu(\boldsymbol{q})$	$\gamma_\mu^{\mathrm{anh}}(\boldsymbol{q})$
1–3	0.0	0.0	0.0	1 and 2	213.5	216.8	0.0
4–6	378.6	376.3	0.1	3 and 4	305.7	306.6	0.1
7–9	1068.7	1036.9	0.2	5 and 6	428.0	431.8	0.6
10–12	1254.5	1214.2	13.3	7 and 8	880.2	849.9	0.9
13–15	1369.5	1332.9	23.3	9 and 10	1122.9	1098.7	0.8
16–18	1645.3	1645.3	34.8	11 and 12	1127.9	1091.4	0.6
19–21	1699.7	1709.3	13.9	13 and 14	1495.7	1468.2	36.7
22 and 23	1703.6	1712.7	4.4	15 and 16	1506.7	1499.9	15.7
24	1789.4	1770.3	3.7	17 and 18	1572.0	1556.2	31.7
				19 and 20	1622.9	1624.4	19.7
				21 and 22	1764.5	1755.5	6.1
				23 and 24	1773.4	1783.8	20.3

C. Superconductivity

The strong anharmonic renormalization of the phonon spectra has a deep impact on the calculated superconducting critical temperatures. We find that calculations based on the harmonic phonon spectrum largely overestimate T_c. We choose typical values for μ^* as 0.10 and 0.15 in the calculations. For a given μ^*, T_c decreases monotonically with increasing pressure both in the harmonic and anharmonic calculations. The suppression of T_c induced by pressure is a consequence of the decrease in the density of states (DOS) at the Fermi level imposed by compression [54], which is suppressed by 35% from 100 GPa to 150 GPa according to our results, as well as the overall hardening of the phonon frequencies. As shown in Fig. 4, for $\mu^* = 0.15$, the resultant T_c values are 7.1, 2.8, and 0.5 K for 109, 125, and 151 GPa, respectively. These results obtained for the $Pm\bar{3}n$ structure using anharmonic phonon frequencies agree well with the electrical resistance experiments [32], which reported that there is no superconducting transition above 4 K in the 120–164 GPa pressure range. If the harmonic phonon spectrum is used instead, T_c values above 4 K are predicted even with the largest value of μ^*, completely contradicting the experimental observation. Our harmonic calculations are in agreement with previous theoretical calculations [32] as using the McMillan equation [51] with $\mu^* = 0.14$ T_c is 21.5 K at about 121 GPa. Indeed, the McMillan equation and the Allen-Dynes modified equation give practically the same T_c. It is worth noting that our DFT calculation may overestimate the DOS at the Fermi level [54], which may lead to an overestimation of the predicted T_c both in the harmonic and anharmonic calculations. However, this overestimation seems insufficient to explain by itself the suppression of the harmonic T_c.

The anharmonic suppression of T_c is a consequence of the clear drop in the electron-phonon coupling constant in the anharmonic limit (see Fig. 4). For example, at 109 GPa (pressure calculated with quantum effects), λ drops from a value of 0.95 down to 0.53, a strong suppression; λ is practically halved. As a result, given $\mu^* = 0.15$, T_c falls from 29 to 7 K, which is equivalent to only 24% of the harmonic result. The suppression is similarly impressive for all studied pressures, whatever the value of μ^* is. The suppression of superconductivity in $Pm\bar{3}n$ AlH_3 is as strong as that estimated for PdH at ambient pressure [37] and PtH at high pressures [33], which crystallize in high-symmetry phases with H atoms in interstitial sites. This suggests that anharmonic suppression

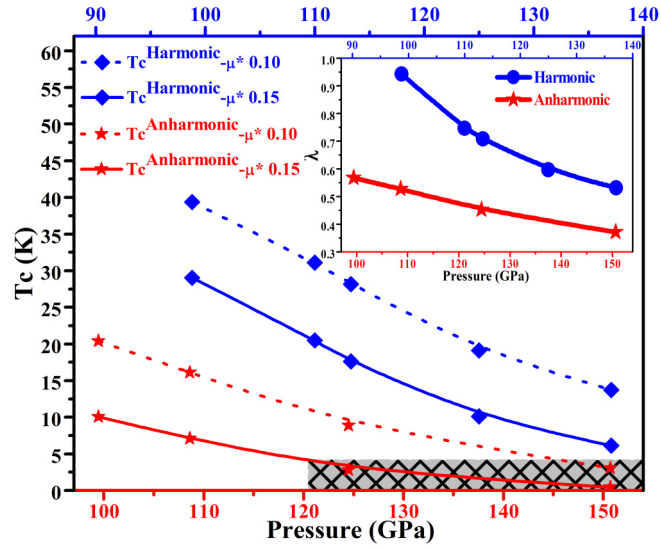

FIG. 4. Superconducting critical temperature T_c and electron-phonon coupling constant λ (inset) as a function of pressure in the harmonic approximation (blue lines) and considering anharmonic effects (red lines). Note that a different pressure scale is used for the harmonic and anharmonic calculations, which includes quantum effects for the latter but not the former. Harmonic and anharmonic results aligned vertically are calculated with the same lattice parameter. T_c calculated with $\mu^* = 0.10$ and 0.15 is plotted with dashed lines and solid lines, respectively. The gray-shaded box marks the pressure region in which no superconductivity was found experimentally above 4 K [32].

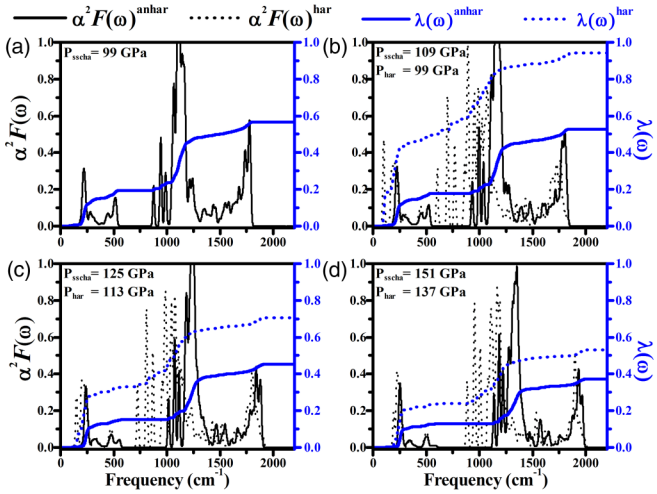

FIG. 5. Anharmonic spectral function $\alpha^2F(\omega)$ (black solid lines) and integrated electron-phonon coupling constant $\lambda(\omega)$ (blue solid lines) at four different quantum pressures: (a) 99 GPa, (b) 109 GPa, (c) 125 GPa, and (d) 151 GPa, respectively. The harmonic results obtained are also shown with dotted lines using the same colors for comparison at three different classical pressures: (b) 99 GPa, (c) 113 GPa, and (d) 137 GPa. The harmonic and anharmonic results in each panel are obtained with the same lattice parameter.

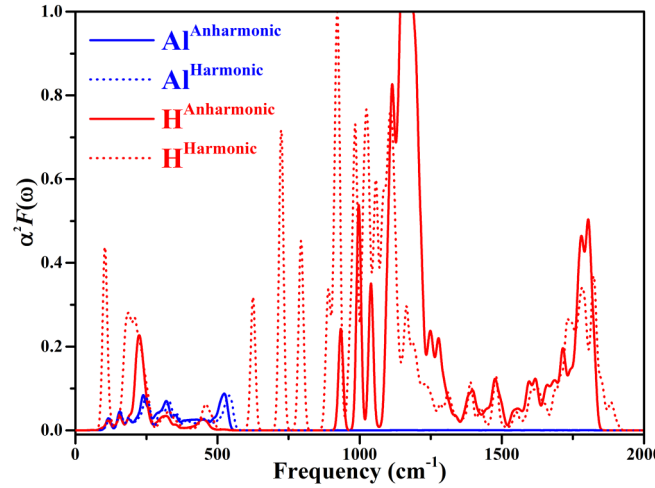

FIG. 6. The projected $\alpha^2F(\omega)$ onto Al and H at the harmonic and anharmonic levels calculated with the same lattice parameter $5.884a_0$, which corresponds in the quantum anharmonic case to 109 GPa. The harmonic results are shown with dotted lines using the same colors for comparison.

of T_c in metallic hydrides with isolated H atoms in interstitial sites may be rather common.

The Eliashberg spectral function $\alpha^2F(\omega)$ and its integral $\lambda(\omega)$, both for anharmonic and harmonic cases, are shown in Fig. 5. It is evident in the figure that while in the anharmonic case the contribution of the low-energy acoustic modes to λ is around 0.2 at all pressures, in the harmonic case it is much larger and it is strongly suppressed by pressure. The reason is that in the harmonic approximation at low pressures there is a significant mixing between H and Al character in the polarization vectors of the acoustic modes. Pressure lifts the frequencies of the H-character modes, reducing effectively the mixing. Anharmonicity also suppresses partly this mixing, and consequently acoustic modes have a weak contribution to λ. This can be seen in Fig. 6, where it is evident that the hydrogen contribution to $\alpha^2F(\omega)$ is suppressed by anharmonicity at low energies. The contribution of each particular atom to the Eliashberg function can be obtained by writing $\alpha^2F(\omega) = \sum_{\bar{a}\bar{b}} \alpha^2F_{\bar{a}\bar{b}}(\omega)$ [$\alpha^2F_{\bar{a}\bar{b}}(\omega)$ can be trivially obtained from Eqs. (12) and (13)]. The partial contributions of Al and H in Fig. 6 are obtained by summing the contributions in $\alpha^2F_{\bar{a}\bar{b}}(\omega)$ of only Al or H atoms, respectively. The large peaks in the harmonic $\alpha^2F(\omega)$ in the 550–1000 cm^{-1} frequency range have a very large contribution to λ and come from the softened modes in the vicinity of the X point (see Fig. 2). This suggests that the softened phonon frequencies at the X point give a large contribution to the electron-phonon coupling. As discussed above, anharmonicity increases these frequencies and, consequently, shifts these peaks to higher energies. As the contribution to λ of a given mode goes as $\lambda_\mu(\boldsymbol{q}) = \gamma_\mu(\boldsymbol{q})/[N(0)\pi\omega^2_\mu(\boldsymbol{q})]$, λ is strongly suppressed by anharmonicity. Due to the small renormalization of other modes beyond the X point, it is reasonable to assume that the bulk of the anharmonic correction to λ and T_c concentrates in the vicinity of X.

The fact that the bulk electron-phonon interaction is concentrated around the X point for the lowest-energy H-character mode is evident when plotting the $\gamma_\mu(\boldsymbol{q})$ linewidth associated with the electron-phonon coupling. In Fig. 7 we show the linewidth calculated following Eq. (13) for the Γ-X, Γ-M, and Γ-R paths at 99 GPa (pressure calculated with quantum anharmonic effects). As depicted, the linewidth associated with the lowest-energy H-character mode largely outweighs the contribution of all the other modes, underlining that this is the mode that contributes the most to λ. This also naturally explains the large anharmonic correction to T_c, as the frequency of this mode is strongly enhanced by anharmonicity.

In our calculations, the electron-phonon contribution to the phonon linewidth of this mode is 90 cm^{-1} at 99 GPa and 89.9 cm^{-1} for 109 GPa, respectively (pressures evaluated including quantum anharmonic effects). This shows that the electron-phonon matrix elements are weakly pressure dependent in this system. For this mode, the electron-phonon contribution to the linewidth is clearly much larger than the anharmonic contribution, which is only 0.9 cm^{-1} (see modes 7 and 8 at the X point in Table I). The electron-phonon contribution to the linewidth is not so large for all the other modes and is comparable (if not smaller) than the anharmonic contribution. Interestingly, even if $\gamma_\mu(\boldsymbol{q})$ does not depend on the phonon frequencies, the electron-phonon linewidth of the strongly renormalized phonon mode at the X point is smaller in the harmonic approximation for the same lattice parameter: 78 cm^{-1}. The explanation for this is the change in the polarization vectors imposed by anharmonicity, which is consistent with the reduction of the H character of the acoustic modes described above. This means that the effect of anharmonicity on the electron-phonon coupling constant and T_c cannot be simply reduced to a renormalization of the phonon frequencies, as it affects them also through a change in the polarization vectors. Since these effects are not trivial and their impact on

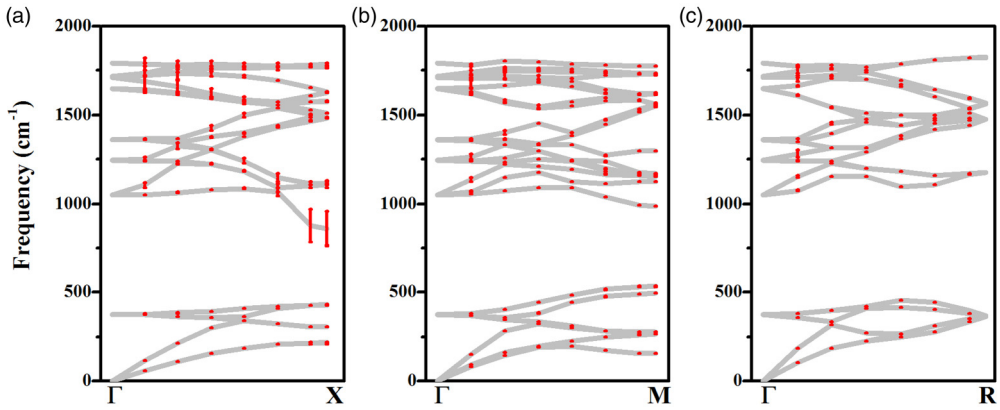

FIG. 7. The linewidth associated with the electron-phonon interaction calculated with the spectra obtained from $\boldsymbol{D}^{(F)}$ for the cubic high-symmetry $Pm\bar{3}n$ phase of AlH_3 at 99 GPa (pressure calculated including quantum effects). (a) Γ-X path, (b) Γ-M path, and (c) Γ-R path. The phonon linewidth is indicated by the size of the red error bars.

T_c cannot be easily anticipated, this motivates the necessity of performing a full nonperturbative anharmonic calculation on hydrides to have reliable results on the electron-phonon coupling effects and superconducting properties.

V. CONCLUSIONS

In summary, in this paper we demonstrate clearly that quantum anharmonic effects are responsible for the absence of superconductivity in $Pm\bar{3}n$ AlH_3 under high pressure, confirming early suggestions [39]. We find that the phonon spectra are strongly affected by anharmonic effects, which leads the structure to be dynamically stable at lower pressures than expected within classical harmonic calculations. Anharmonicity reduces the electron-phonon coupling constant by no less than 30% and T_c by at least 59% in the range of 109–151 GPa. The bulk of the anharmonic correction, as well as the electron-phonon interaction, concentrates around the zone border X point. The $Pm\bar{3}n$ remains metastable (because dynamically stable) below 100 GPa, opening the possibility of its synthesis below this pressure. Our work underlines that superconducting properties of hydrides at high pressure can only be properly described by including quantum and anharmonic effects.

ACKNOWLEDGMENTS

This research was supported by the European Research Council (ERC) under the European Union's Horizon 2020 research and innovation program (Grant Agreement No. 802533). R.B. thankfully acknowledges the computer resources at Altamira and the technical support provided by Physics Institute of Cantabria (IFCA) (RES-FI-2020-3-0028).

[1] N. W. Ashcroft, Phys. Rev. Lett. **21**, 1748 (1968).
[2] J. A. Flores-Livas, L. Boeri, A. Sanna, G. Profeta, R. Arita, and M. Eremets, Phys. Rep. **856**, 1 (2020).
[3] T. Bi, N. Zarifi, T. Terpstra, and E. Zurek, *Reference Module in Chemistry, Molecular Sciences and Chemical Engineering* (Elsevier, New York, 2019), pp. 1–36.
[4] C. J. Pickard, I. Errea, and M. I. Eremets, Annu. Rev. Condens. Matter Phys. **11**, 57 (2020).
[5] G. Gao, A. R. Oganov, A. Bergara, M. Martinez-Canales, T. Cui, T. Iitaka, Y. Ma, and G. Zou, Phys. Rev. Lett. **101**, 107002 (2008).
[6] M. Martinez-Canales, A. R. Oganov, Y. Ma, Y. Yan, A. O. Lyakhov, and A. Bergara, Phys. Rev. Lett. **102**, 087005 (2009).
[7] G. Gao, A. R. Oganov, P. Li, Z. Li, H. Wang, T. Cui, Y. Ma, A. Bergara, A. O. Lyakhov, T. Iitaka, and G. Zou, Proc. Natl. Acad. Sci. USA **107**, 1317 (2010).
[8] D. Y. Kim, R. H. Scheicher, C. J. Pickard, R. J. Needs, and R. Ahuja, Phys. Rev. Lett. **107**, 117002 (2011).
[9] H. Wang, J. S. Tse, K. Tanaka, T. Iitaka, and Y. Ma, Proc. Natl. Acad. Sci. USA **109**, 6463 (2012).
[10] D. C. Lonie, J. Hooper, B. Altintas, and E. Zurek, Phys. Rev. B **87**, 054107 (2013).
[11] D. Duan, Y. Liu, F. Tian, D. Li, X. Huang, Z. Zhao, H. Yu, B. Liu, W. Tian, and T. Cui, Sci. Rep. **4**, 6968 (2014).
[12] D. Duan, X. Huang, F. Tian, D. Li, H. Yu, Y. Liu, Y. Ma, B. Liu, and T. Cui, Phys. Rev. B **91**, 180502(R) (2015).
[13] Y. Li, J. Hao, H. Liu, J. S. Tse, Y. Wang, and Y. Ma, Sci. Rep. **5**, 9948 (2015).
[14] S. Zhang, Y. Wang, J. Zhang, H. Liu, X. Zhong, H.-F. Song, G. Yang, L. Zhang, and Y. Ma, Sci. Rep. **5**, 15433 (2015).
[15] H. Liu, Y. Li, G. Gao, J. S. Tse, and I. I. Naumov, J. Phys. Chem. C **120**, 3458 (2016).
[16] X. Zhong, H. Wang, J. Zhang, H. Liu, S. Zhang, H.-F. Song, G. Yang, L. Zhang, and Y. Ma, Phys. Rev. Lett. **116**, 057002 (2016).
[17] F. Peng, Y. Sun, C. J. Pickard, R. J. Needs, Q. Wu, and Y. Ma, Phys. Rev. Lett. **119**, 107001 (2017).
[18] H. Liu, I. I. Naumov, R. Hoffmann, N. W. Ashcroft, and R. J. Hemley, Proc. Natl. Acad. Sci. USA **114**, 6990 (2017).
[19] Y. Sun, J. Lv, Y. Xie, H. Liu, and Y. Ma, Phys. Rev. Lett. **123**, 097001 (2019).

[20] W. Cui, T. Bi, J. Shi, Y. Li, H. Liu, E. Zurek, and R. J. Hemley, Phys. Rev. B **101**, 134504 (2020).
[21] Y. Sun, Y. Tian, B. Jiang, X. Li, H. Li, T. Iitaka, X. Zhong, and Y. Xie, Phys. Rev. B **101**, 174102 (2020).
[22] M. Borinaga, I. Errea, M. Calandra, F. Mauri, and A. Bergara, Phys. Rev. B **93**, 174308 (2016).
[23] M. Borinaga, J. Ibañez-Azpiroz, A. Bergara, and I. Errea, Phys. Rev. Lett. **120**, 057402 (2018).
[24] R. P. Dias and I. F. Silvera, Science **355**, 715 (2017).
[25] A. P. Drozdov, M. I. Eremets, I. A. Troyan, V. Ksenofontov, and S. I. Shylin, Nature (London) **525**, 73 (2015).
[26] M. Somayazulu, M. Ahart, A. K. Mishra, Z. M. Geballe, M. Baldini, Y. Meng, V. V. Struzhkin, and R. J. Hemley, Phys. Rev. Lett. **122**, 027001 (2019).
[27] A. P. Drozdov, P. P. Kong, V. S. Minkov, S. P. Besedin, M. A. Kuzovnikov, S. Mozaffari, L. Balicas, F. F. Balakirev, D. E. Graf, V. B. Prakapenka, E. Greenberg, D. A. Knyazev, M. Tkacz, and M. I. Eremets, Nature (London) **569**, 528 (2019).
[28] I. A. Troyan, D. V. Semenok, A. G. Kvashnin, A. V. Sadakov, O. A. Sobolevskiy, V. M. Pudalov, A. G. Ivanova, V. B. Prakapenka, E. Greenberg, A. G. Gavriliuk, I. S. Lyubutin, V. V. Struzhkin, A. Bergara, I. Errea, R. Bianco, M. Calandra, F. Mauri, L. Monacelli, R. Akashi, and A. R. Oganov, Adv. Mater. **33**, 2006832 2021.
[29] E. Snider, N. Dasenbrock-Gammon, R. McBride, X. Wang, N. Meyers, K. V. Lawler, E. Zurek, A. Salamat, and R. P. Dias, Phys. Rev. Lett. **126**, 117003 (2021).
[30] P. P. Kong, V. S. Minkov, M. A. Kuzovnikov, S. P. Besedin, A. P. Drozdov, S. Mozaffari, L. Balicas, F. F. Balakirev, V. B. Prakapenka, E. Greenberg, D. A. Knyazev, and M. I. Eremets, arXiv:1909.10482.
[31] E. Snider, N. Dasenbrock-Gammon, R. McBride, M. Debessai, H. Vindana, K. Vencatasamy, K. V. Lawler, A. Salamat, and R. P. Dias, Nature (London) **586**, 373 (2020).
[32] I. Goncharenko, M. I. Eremets, M. Hanfland, J. S. Tse, M. Amboage, Y. Yao, and I. A. Trojan, Phys. Rev. Lett. **100**, 045504 (2008).
[33] I. Errea, M. Calandra, and F. Mauri, Phys. Rev. B **89**, 064302 (2014).
[34] I. Errea, M. Calandra, C. J. Pickard, J. Nelson, R. J. Needs, Y. Li, H. Liu, Y. Zhang, Y. Ma, and F. Mauri, Phys. Rev. Lett. **114**, 157004 (2015).
[35] I. Errea, M. Calandra, C. J. Pickard, J. R. Nelson, R. J. Needs, Y. Li, H. Liu, Y. Zhang, Y. Ma, and F. Mauri, Nature (London) **532**, 81 (2016).
[36] I. Errea, F. Belli, L. Monacelli, A. Sanna, T. Koretsune, T. Tadano, R. Bianco, M. Calandra, R. Arita, F. Mauri, and J. A. Flores-Livas, Nature (London) **578**, 66 (2020).
[37] I. Errea, M. Calandra, and F. Mauri, Phys. Rev. Lett. **111**, 177002 (2013).
[38] C. J. Pickard and R. J. Needs, Phys. Rev. B **76**, 144114 (2007).
[39] B. Rousseau and A. Bergara, Phys. Rev. B **82**, 104504 (2010).
[40] I. Errea, Eur. Phys. J. B **89**, 237 (2016).
[41] R. Bianco, I. Errea, L. Paulatto, M. Calandra, and F. Mauri, Phys. Rev. B **96**, 014111 (2017).
[42] L. Monacelli, I. Errea, M. Calandra, and F. Mauri, Phys. Rev. B **98**, 024106 (2018).
[43] L. Monacelli, R. Bianco, M. Cherubini, M. Calandra, I. Errea, and F. Mauri, arXiv:2103.03973.
[44] L. Monacelli and F. Mauri, Phys. Rev. B **103**, 104305 (2021).
[45] J.-M. Lihm and C.-H. Park, arXiv:2010.15725.
[46] R. Bianco, I. Errea, M. Calandra, and F. Mauri, Phys. Rev. B **97**, 214101 (2018).
[47] P. B. Allen and R. C. Dynes, Phys. Rev. B **12**, 905 (1975).
[48] P. Morel and P. W. Anderson, Phys. Rev. **125**, 1263 (1962).
[49] P. Giannozzi, S. Baroni, N. Bonini, M. Calandra, R. Car, C. Cavazzoni, D. Ceresoli, G. L. Chiarotti, M. Cococcioni, I. Dabo, A. Dal Corso, S. de Gironcoli, S. Fabris, G. Fratesi, R. Gebauer, U. Gerstmann, C. Gougoussis, A. Kokalj, M. Lazzeri, L. Martin-Samos *et al.*, J. Phys.: Condens. Matter **21**, 395502 (2009).
[50] P. Giannozzi, O. Andreussi, T. Brumme, O. Bunau, M. B. Nardelli, M. Calandra, R. Car, C. Cavazzoni, D. Ceresoli, M. Cococcioni, N. Colonna, I. Carnimeo, A. Dal Corso, S. de Gironcoli, P. Delugas, R. A. DiStasio, Jr., A. Ferretti, A. Floris, G. Fratesi, G. Fugallo *et al.*, J. Phys.: Condens. Matter **29**, 465901 (2017).
[51] D. Vanderbilt, Phys. Rev. B **41**, 7892 (1990).
[52] J. P. Perdew, K. Burke, and M. Ernzerhof, Phys. Rev. Lett. **77**, 3865 (1996).
[53] S. Baroni, S. de Gironcoli, A. Dal Corso, and P. Giannozzi, Rev. Mod. Phys. **73**, 515 (2001).
[54] M. Geshi and T. Fukazawa, Physica B (Amsterdam) **411**, 154 (2013).